

# Changes in Small Intestinal Homeostasis, Morphology, and Gene Expression during Rotavirus Infection of Infant Mice

Jos A. Boshuizen,<sup>1</sup> Johan H. J. Reimerink,<sup>2</sup> Anita M. Korteland-van Male,<sup>1</sup>  
Vanessa J. J. van Ham,<sup>1</sup> Marion P. G. Koopmans,<sup>2</sup> Hans A. Büller,<sup>1</sup>  
Jan Dekker,<sup>1</sup> and Alexandra W. C. Einerhand<sup>1\*</sup>

*Laboratory of Pediatrics, Pediatric Gastroenterology, and Nutrition, Erasmus MC/ Sophia, Rotterdam,<sup>1</sup> and  
Research Laboratory for Infectious Diseases, National Institute for Public Health and the Environment,  
Bilthoven,<sup>2</sup> The Netherlands*

Received 13 May 2003/Accepted 5 September 2003

**Rotavirus is the most important cause of infantile gastroenteritis. Since in vivo mucosal responses to a rotavirus infection thus far have not been extensively studied, we related viral replication in the murine small intestine to alterations in mucosal structure, epithelial cell homeostasis, cellular kinetics, and differentiation. Seven-day-old suckling BALB/c mice were inoculated with  $2 \times 10^4$  focus-forming units of murine rotavirus and were compared to mock-infected controls. Diarrheal illness and viral shedding were recorded, and small intestinal tissue was evaluated for rotavirus (NSP4 and structural proteins)- and enterocyte-specific (lactase, SGLT1, and L-FABP) mRNA and protein expression. Morphology, apoptosis, proliferation, and migration were evaluated (immuno)histochemically. Diarrhea was observed from days 1 to 5 postinfection, and viral shedding was observed from days 1 to 10. Two peaks of rotavirus replication were observed at 1 and 4 days postinfection. Histological changes were characterized by the accumulation of vacuolated enterocytes. Strikingly, the number of vacuolated cells exceeded the number of cells in which viral replication was detectable. Apoptosis and proliferation were increased from days 1 to 7, resulting in villous atrophy. Epithelial cell turnover was significantly higher (<4 days) than that observed in controls (7 days). Since epithelial renewal occurred within 4 days, the second peak of viral replication was most likely caused by infection of newly synthesized cells. Expression of enterocyte-specific genes was downregulated in infected cells at mRNA and protein levels starting as early as 6 h after infection. In conclusion, we show for the first time that rotavirus infection induces apoptosis in vivo, an increase in epithelial cell turnover, and a shutoff of gene expression in enterocytes showing viral replication. The shutoff of enterocyte-specific gene expression, together with the loss of mature enterocytes through apoptosis and the replacement of these cells by less differentiated dividing cells, likely leads to a defective absorptive function of the intestinal epithelium, which contributes to rotavirus pathogenesis.**

Rotaviruses are one of the most significant causes of gastroenteritis, malnutrition, and diarrhea in young children and animals (17, 28). Mortality rates are low in developed countries, where illness is usually self-limiting (64). However, each year more than 600,000 young children die in developing countries throughout the world (26). Rotavirus infection in children is mainly restricted to the small intestinal villus epithelium, resulting in the occurrence of total villus atrophy (3). Although rotavirus can infect older children and adults, diarrheal disease is primarily observed in children under 2 years of age (16, 17, 28).

Rotavirus-induced diarrhea is thought to be caused by a combination of factors (55), which include a reduction in epithelial surface area, replacement of mature enterocytes by immature (crypt-like) cells (43), an osmotic effect resulting from incomplete absorption of carbohydrates from the intestinal lumen in combination with bacterial fermentation of these nonabsorbed compounds, secretion of intestinal fluid

and electrolytes through activation of the enteric nervous system (37), and the effect of the rotavirus nonstructural protein 4 (NSP4), which is thought to act as a viral enterotoxin (1).

Since the epithelium is the primary target of rotavirus infection, epithelial dysfunction plays an important role in rotavirus pathogenesis. However, thus far, in vivo data concerning specific epithelial responses are rather limited (10, 22, 29, 43, 53, 57). Studies of the effect of infection on epithelial homeostasis in vivo are mainly restricted to studies of piglets, young rabbits, and mice (10, 22, 29, 57).

In piglets, sucrase-isomaltase activity was found to be decreased, whereas thymidine kinase activity was increased during rotavirus infection (57). In rabbits, rotavirus infection was shown to impair epithelial homeostasis, and intestinal brush border membrane  $\text{Na}^+$  solute cotransport activities were affected (21, 22). In young mice, homologous rotavirus infection affects the small intestinal epithelium by reducing leucine uptake and lactase and alkaline phosphatase activities, whereas the maturation of sucrase-isomaltase activity was found to be precocious (10, 29).

Vacuolization of enterocytes during rotavirus infection is observed in mice and rats (8, 42, 43) but is not a feature of rotavirus infection in calves, lambs, and piglets (41, 57, 59).

\* Corresponding author. Mailing address: Laboratory of Pediatrics, Pediatric Gastroenterology and Nutrition, Erasmus MC, Rm. Ee1571A, Dr. Molewaterplein 50, 3015 GE Rotterdam, The Netherlands. Phone: (31)-10-4087444. Fax: (31)-10-4089486. E-mail: a.einerhand@erasmusmc.nl.

These differences have been attributed to the specific nature of the host response and not to the virus, since vacuolization is also a characteristic feature of heterologous infections in mice (2, 19, 38). Mice usually do not develop any symptoms beyond 2 weeks of age, and infection of adult mice occurs without disease or histopathological lesions (7, 18, 43, 46, 61, 67).

The present study was designed to get more insight into the pathogenesis of rotavirus infection by studying epithelial homeostasis and dysfunction during rotavirus infection in mice. We examined the induction of diarrheal illness and timing and extent of rotavirus replication in the murine small intestine, and we related viral replication to alterations in mucosal structure, epithelial homeostasis, kinetics, and differentiation.

## MATERIALS AND METHODS

**Animals.** Pregnant dams were obtained from Harlan (Zoetermeer, The Netherlands). Dams, either with their control or inoculated litters, were housed in microisolator cages under negative pressure in a specific-pathogen-free environment. Chicken-protein-free rodent chow [9605/9608; Harlan Teklad TRM (A)] and deionized water were autoclaved and provided *ad libitum* until the end of the experiment. All dams were rotavirus antibody negative as measured by enzyme-linked immunosorbent assay (ELISA) (as described below). All the experiments were performed with the approval of the Animal Studies Ethics Committee of the National Institute of Public Health and the Environment.

**Virus.** The EDIM (epizootic diarrhea of infant mice) mouse rotavirus strain was obtained from R. Ward, Children's Hospital Research Foundation, Cincinnati, Ohio (40). The strain used is an unpassaged virus isolated directly from the stools of ill mice.

**Virus inoculations and subsequent animal-handling procedures.** Seven-day-old BALB/c mice were inoculated intragastrically with  $2 \times 10^4$  focus-forming units (FFU) of the EDIM rotavirus strain. Control mice were mock infected through inoculation with phosphate-buffered saline (PBS). To analyze epithelial proliferative kinetics, 5-bromo-2'-deoxyuridine (BrdU) (30 mg/kg of body weight; Sigma, St. Louis, Mo.) was injected intraperitoneally just before inoculation. After inoculation and injection of BrdU, the mice were returned to their mothers and allowed to suckle. After 6 h and at days 1, 2, 4, 7, 10, and 14, five infected and three control mice were sacrificed per time point. Segments of jejunum (anatomic middle of the small intestine) and ileum (distal 2 cm of the small intestine) were rinsed in PBS and fixed for 4 h in 4% (wt/vol) paraformaldehyde (Merck, Darmstadt, Germany) dissolved in PBS. The segments were then dehydrated through a graded series of ethanol and xylene (Merck) and embedded in Paraplast Plus (Sherwood Medical, Den Bosch, The Netherlands) as previously described (66). In addition, adjacent segments of the jejunum and ileum were dissected and snap frozen in liquid nitrogen and stored at  $-80^\circ\text{C}$  for RNA and protein isolation.

**Detection of rotavirus in stools.** To determine rotavirus shedding, fecal samples were collected from each individual sacrificed mouse at 0 to 14 days postinfection (dpi) and stored at  $-20^\circ\text{C}$ . Samples were then homogenized in PBS in a 10% (wt/vol) solution or suspension and centrifuged ( $1,000 \times g$  for 5 min) to remove debris before being analyzed. The presence of rotavirus antigen in fecal samples was determined by ELISA using the Premier Rotaclone kit (Meridian Diagnostics, Cincinnati, Ohio). The test was considered positive if the optical density at 450 nm ( $\text{OD}_{450}$ ) of the well containing stool minus the  $\text{OD}_{450}$  of control wells was  $\geq 0.1$ .

**Diarrhea score.** The severity of diarrheal illness was assessed by examination of fecal material. Stools were scored from 1 to 4 based on color, texture, and amount. Normal feces were given a score of 1, exceptionally loose feces were given a score of 2, loose yellow-green feces were given a score of 3, and watery feces were given a score of 4. Stools with a score of  $\geq 2$  were considered to be diarrhea. The percentage of diarrhea was calculated by dividing the number of diarrheic samples by the total number of mice scored for diarrhea each day. Mice from which no stool could be obtained were considered as mice with no diarrhea. The diarrhea severity was determined by dividing the sum of all scores by the number of total stool samples collected each day.

**Antibody production.** Polyclonal rabbit hyperimmune sera were raised against cesium chloride-purified simian rotavirus (SA11) or a synthetic peptide corresponding to amino acids 114 to 135 of NSP4 from the SA11 strain (KLTT REIEQVELLKRIYDKLTV). The NSP4 peptide was coupled to keyhole limpet hemocyanin using the EDC kit from Pierce (Rockford, Ill.), following the man-

ufacturer's protocol. Purified rotavirus or the NSP4 peptide was emulsified with Freund's adjuvant and injected subcutaneously into rabbits following the method we have described previously (63). The polyclonal serum raised against purified rotavirus was used for quantifying rotavirus protein in intestinal homogenates. The polyclonal serum raised against the NSP4 peptide was used for immunohistochemistry.

**Histology and morphometry.** For standard histochemical staining or immunohistochemistry, paraffin-embedded tissues were sectioned (5  $\mu\text{m}$ ), deparaffinized with xylene (Merck), and rehydrated in graded ethanol solutions as previously described (49). Epithelial morphology was analyzed after staining with Gill's hematoxylin (Vector Laboratories, Burlingame, Calif.) and eosin (Merck). Crypt depth and villus height were measured manually in well-oriented sections (10 measurements per region per mouse) using a micrometer (Nikon, Bunnik, The Netherlands) mounted in an Eclipse E600 Microscope (Nikon). By dividing the crypt-villus axis into five equal regions, the positions of vacuolated cells and cells containing replicating virus along the crypt-villus axis were assessed. The positions were scored from 1 to 5, representing the tips of the villi to the crypts, respectively. The presence of vacuoles was judged by standard hematoxylin-eosin staining. The vacuoles were examined for the presence of acid and neutral carbohydrates using a combined alcian blue-periodic acid-Schiff (PAS) stain. The presence of replicating virus was determined by immunohistochemistry using the antibody against NSP4 (see below). Ten crypt-villus units per segment of the small intestine per animal were analyzed. All scores were averaged per intestinal segment per animal and were subsequently averaged between animals to calculate the mean score per segment per time point ( $\pm$  standard error of the mean [SEM]).

**Immunohistochemistry.** Deparaffinized and rehydrated sections were incubated overnight at  $4^\circ\text{C}$  using the primary mouse monoclonal antibodies anti-human proliferating-cell nuclear antigen (PCNA) (1:1,500; Boehringer), anti-BrdU (1:250; Boehringer), and anti-rat lactase (1:1,000; provided by A. Quaroni [45]) or the rabbit polyclonal antibodies anti-(cleaved) caspase-3 (1:500; Cell Signaling Technology, Beverly, Mass.), anti-NSP4 (1:1,000), anti-rat liver fatty acid binding protein (L-FABP) (1:2,000; provided by J. Gordon [54]), or anti-rabbit sodium glucose cotransporter 1 (SGLT1) (1:1,000; provided by B. A. Hirayama et al. [24]). Immunohistochemistry was carried out as described previously (49).

**Epithelial proliferation and apoptosis.** The effects of rotavirus infection on intestinal epithelial cell migration kinetics were analyzed through detection of BrdU, a nucleotide analog that is incorporated into the DNA of proliferating cells. At different time points after injection of BrdU, the positions of the foremost and least-advanced BrdU-labeled cells in 10 crypt-villus units per animal were expressed as the number of cell positions from the crypt-villus axis. Proliferating (PCNA-positive) and apoptotic (caspase-3-positive) cells were counted in villi and crypts of the jejunum until 14 dpi, of, respectively, 10 and 30 well-oriented crypt-villus units per animal per time point.

**In situ hybridization and probe preparation.** Nonradioactive in situ hybridization was performed using the method as previously described (34, 49). Digoxigenin (DIG)-11-UTP labeled RNA probes were prepared according to the manufacturer's protocol (Boehringer Mannheim GmbH, Mannheim, Germany) using T3, T7, or SP6 RNA polymerase. The following probes were used: a 1-kb *NcoI* fragment based on a 2.4-kb rat SGLT1 cDNA ligated in pBluescript (11), a 350-bp fragment of rat L-FABP cDNA ligated in pBluescript (58), a 250-bp *EcoRI/HindIII* mouse beta-actin fragment ligated in pSP65 (32), and a 750-bp *NcoI/SmaI* NSP4 (SA11 strain) fragment ligated in pBluescript (see below). Transcripts longer than 450 bp were hydrolyzed in 80 mM  $\text{NaHCO}_3$  and 120 mM  $\text{Na}_2\text{CO}_3$ , pH 10.2, to obtain probes with various lengths of  $\leq 450$  bp (12).

**Quantitation of mRNA.** Total RNA was isolated from frozen small intestinal segments, using Trizol reagent (Gibco-BRL, Gaithersburg, Md.), following the manufacturer's protocol. Integrity of the RNA was assessed by visual analysis of the 28S and 18S rRNAs after electrophoresis and staining with ethidium bromide. Subsequently, 1  $\mu\text{g}$  of total RNA was dot blotted on Hybond-N<sup>+</sup> (Amersham, Little Chalfont, Buckinghamshire, England) using a vacuum-operated manifold (BioDot; Bio-Rad, Hercules, Calif.). All blots were hybridized using specific  $^{32}\text{P}$ -labeled cDNA probes as described previously (66). To correct for the amount of RNA that was spotted, hybridized signals were corrected for glyceraldehyde-3-phosphate dehydrogenase (GAPDH) mRNA expression using a 1.4-kb human GAPDH probe (66). Hybridization signals were measured through autoradiography using a PhosphorImager and ImageQuant software (Molecular Imaging, Sunnyvale, Calif.). The following probes were used: a 394-bp *NcoI* fragment of rat SGLT1 (obtained from Charles Burant), a 400-bp *XhoI/EcoRI* fragment of rat L-FABP (58), and a 1.8-kb *EcoRI* fragment of rat lactase (6). For the construction of the NSP4 probe, reverse transcription-PCR was performed on RNA from simian rotavirus (SA11 strain)-infected MA104 monkey kidney

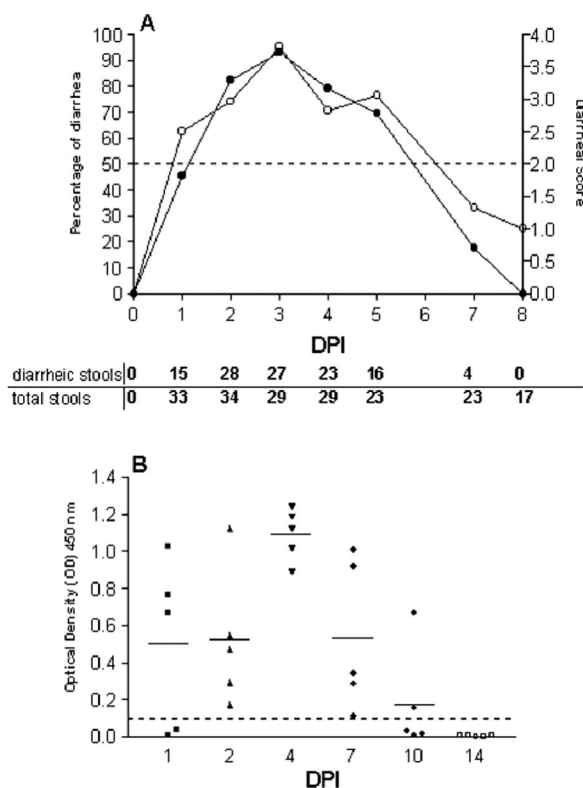


FIG. 1. Percentage of diarrhea (●) and mean diarrheal score (○) (A) and viral antigen shedding (B) in neonatal mice inoculated with rotavirus. Percentage of diarrhea per day was calculated by dividing the number of diarrheic samples by the number of total samples collected each day. A score of  $\geq 2$  was considered diarrhea, whereas a score of  $< 2$  was considered normal. The mean diarrheal score was determined by dividing the sum of all diarrhea or not-diarrhea scores (1 to 4) by the number of total samples scored each day (numbers are listed at the bottom of the figure). Fecal samples ( $n = 5$  per day) from 0 to 14 dpi were assayed for rotavirus antigen shedding by ELISA (B). Data are expressed as net and mean OD<sub>450</sub> and represent individual values obtained for fecal samples. Readings of  $\geq 0.1$  are considered positive.

cells. NSP4 was cloned using the primers GGAACCATGGAAAAGCTTACCG ACCTC (nucleotides 46 to 62) and TCCCCGGGTACATTAAGACCGT TCCT (nucleotides 730 to 750), based on the NSP4 SA11 coding sequence (5). PCR fragments were cloned into the *EcoRI* sites of PCR 2.1 (Invitrogen).

**Quantitation of rotavirus protein.** Proteins were isolated from frozen segments by homogenization of the tissue in 500  $\mu$ l of (Tris-) homogenization buffer containing Triton X-100 (BDH, Poole, England), 1% sodium dodecyl sulfate, and various protease inhibitors as previously described (48). Protein concentration was measured using a bicinchoninic acid protein assay reagent kit (Pierce). Bovine serum albumin was used as a standard. To quantify rotavirus structural protein contents, protein homogenates were dot blotted on nitrocellulose (Nitran; Schleicher & Schuell, Dassell, Germany). The blots were blocked for 1 h with blocking buffer (50 mM Tris-HCl [pH 7.8], 5% [wt/vol] nonfat dry milk powder [Lyempf, Kampen, The Netherlands], 2 mM  $\text{CaCl}_2$ , 0.05% [vol/vol] Nonidet P-40 [BDH], 0.01% [vol/vol] antifoam [Sigma]) and incubated for 18 h with rabbit hyperimmune serum raised against SA11 rotavirus particles (1:1,000). After being washed in blocking buffer, the blots were incubated with  $^{125}\text{I}$ -labeled protein A (specific activity, 33.8 mCi/mg; Amersham) for 2 h. Bound  $^{125}\text{I}$ -labeled protein A was then detected and the elicited signals were quantified using a PhosphorImager and ImageQuant software (Molecular Imaging).

**Statistical analysis.** Statistical analysis of all data from control and infected groups was performed using Student's *t* test for unpaired data (two tailed). To compare three or more groups, data were analyzed by analysis of variance

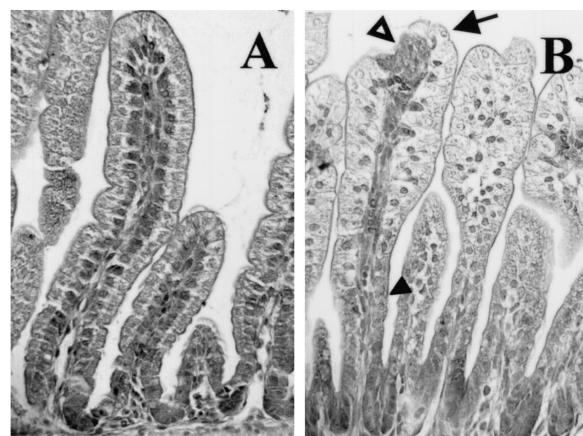


FIG. 2. Histopathological lesions in mouse small intestine (jejunum) during rotavirus infection at 1 dpi. Sections were stained with hematoxylin and eosin. (A) In control animals, enterocytes were clearly polarized and the nuclei were localized at the base of the enterocytes. (B) In infected mice at 1 dpi, histopathological changes were characterized by vacuolization of the enterocytes, swelling of the villus tips (arrow), constriction of the bases, and nuclei that were irregularly positioned within the cells (solid arrowhead). In many villi, lesions seemed to be present at the tips (open arrowhead). Magnification,  $\times 250$ .

followed by an unpaired *t* test. Data were expressed as the mean  $\pm$  SEM, and *P* values of  $\leq 0.05$  were considered statistically significant.

## RESULTS

**Rotavirus infection of 7-day-old mice caused diarrhea and virus shedding starting at 1 dpi.** To be able to study rotavirus infection in vivo, 7-day-old suckling mice were inoculated orally with  $2 \times 10^4$  FFU of EDIM rotavirus. As a control, mice of the same age were inoculated with PBS. Control mice did not develop diarrhea at any time point and did not shed rotavirus antigen over a period of 14 days after PBS inoculation as measured by ELISA (data not shown). Mice inoculated with rotavirus developed diarrhea over a period of 5 days (Fig. 1A). The onset of diarrhea occurred as early as 1 day postinfection (dpi). The highest percentage of diarrhea occurred at 3 dpi, reaching 93% (Fig. 1A). At this time point also the severity of diarrheal illness was maximal. The duration of viral antigen shedding was maximally 10 days (Fig. 1B). At 1 dpi three of the five animals examined shed virus, and at 4 dpi viral shedding was maximal. At 10 dpi only two of five examined animals were still shedding virus. None of the infected mice died spontaneously. Thus, the onset of diarrhea occurred approximately at the same time as viral antigen shedding began.

**Histopathological lesions in mouse small intestine during rotavirus infection.** At necropsy, accumulation of fluid in the small intestine was observed in infected mice. This was first observed at 1 dpi, persisted through 4 dpi, and was accompanied by distention of the ileum and large intestine. At these time points the diameter of the duodenum of infected mice, however, appeared smaller than that of the controls (data not shown). In control animals, jejunal enterocytes were clearly polarized and the nuclei were localized at the base of the enterocytes (Fig. 2A). Histopathological changes in the small intestine of rotavirus-infected mice were characterized by swol-



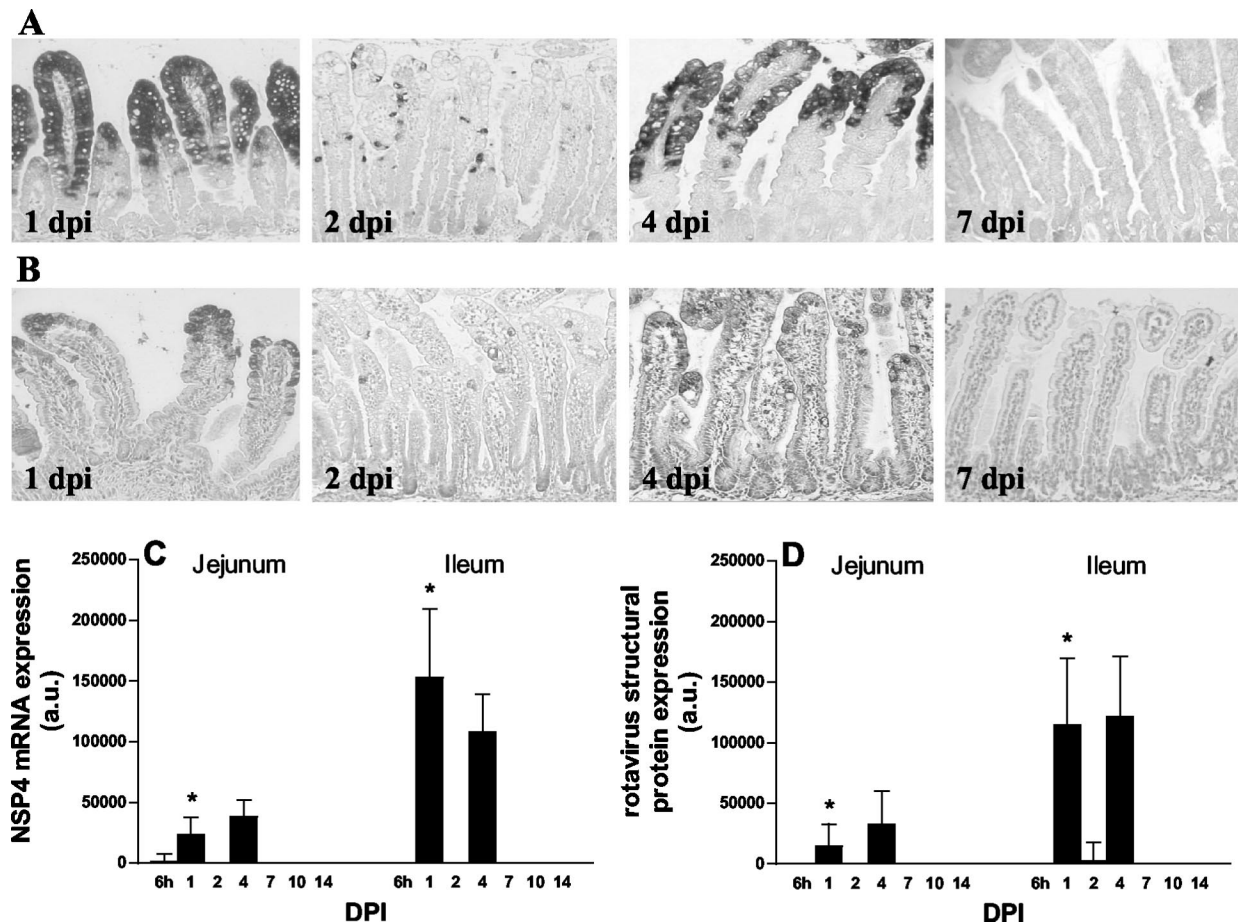


FIG. 3. Kinetics of rotavirus replication in the mouse small intestine. Levels of NSP4 mRNA (A) and protein (B) expression in jejunum at several days postinfection were determined by in situ hybridization and immunohistochemistry, respectively. No rotavirus antigen was detected beyond 7 dpi in any part of the small intestinal epithelium. Quantitative expression of NSP4 mRNA and structural rotavirus proteins were analyzed by RNA and protein dot blotting, respectively (C and D). At 1 dpi, the levels of NSP4 mRNA and structural protein expression were significantly higher in the ileum than in the jejunum. \*,  $P < 0.05$  (Student's  $t$  test). Magnification,  $\times 150$ . Error bars, SEM; a.u., arbitrary units.

len villus tips and constricted villus bases. In many villi, lesions seemed to be present at the tips (Fig. 2B). In infected mice at 1 dpi, nuclei were enlarged and irregularly positioned within the cells. At the constricted bases of the jejunal villi, the cells were flattened and rounded (Fig. 2B). During infection, large vacuoles occurred in the enterocytes lining most of the surface of the villi in the small intestine (Fig. 2B). Particularly in the ileum, accumulation of supranuclear vacuoles was observed, while in the duodenum histological changes were mainly restricted to rounding of enterocytes (data not shown). Vacuolization was observed from 1 to 7 dpi and was most pronounced in the ileum at 2 dpi. Almost-complete resolution of the histopathological changes was observed by 7 dpi. At the start of the weaning period at 10 dpi, when the pups were 17 days old, minimal vacuolization was noticeable at the tips of the villi in (formerly) infected and control animals. These vacuoles, however, were only detected in the ileum and were morphologically different from and always far fewer in number than the vacuoles observed in the inoculated mouse pups before 7 dpi (data not shown). The vacuoles observed during infection and during the start of the weaning period did not stain for acid or

neutral carbohydrates with a combined alcian blue-PAS stain (data not shown).

**Kinetics of rotavirus replication in the mouse small intestine.** To determine the kinetics of rotavirus replication in young mice, the presence of replicating virus in small intestinal tissue was determined by detection of rotavirus structural proteins and NSP4. NSP4 is not found in mature infectious virus particles and is only synthesized within host cells during virus replication. The presence of NSP4 is therefore an incontrovertible indication for viral replication. At 6 h postinfection (hpi), NSP4 was detected at RNA and protein levels in an occasional epithelial cell in the duodenum and jejunum of infected mice, as observed by in situ hybridization and immunohistochemistry, respectively (data not shown). At 1 dpi rotavirus NSP4 protein and mRNA were detected in almost all the epithelial cells located in the upper part of the small intestinal villi of rotavirus infected mice (Fig. 3A and B, jejunum). At 2 dpi, when vacuolated cells were still abundantly present, NSP4 expression was only detected in a few cells in the villus epithelium. At 4 dpi, a second peak of rotavirus replication was observed (Fig. 3A and B). No rotavirus antigen was

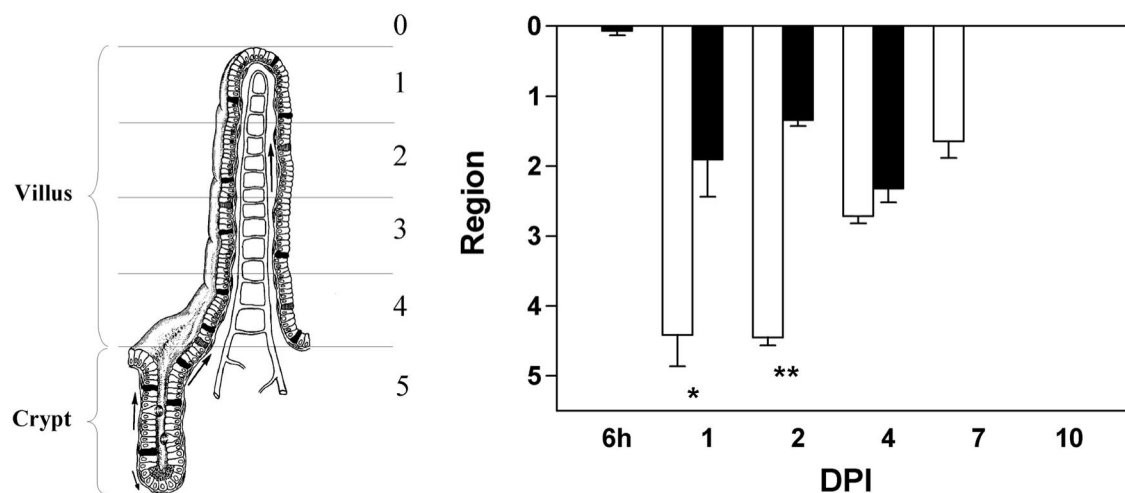


FIG. 4. The pattern of epithelial vacuolization is more extensive than the pattern of replicating virus. Crypt-villus units in the jejunum were divided into five regions of equal length (see the left part of the figure). The position of the vacuolated cells (open bars) and virus-containing cells (solid bars) on the crypt-villus axis was scored from 1 to 5, representing the regions from the tips of the villi to the crypts. At 1 and 2 dpi, infected cells were exclusively found in the upper part of the villi, whereas vacuolated cells were observed along the entire villi and even at the base of the villi. Values are means + SEM (error bars). \* and \*\*,  $P < 0.01$  and  $P < 0.001$ , respectively (Student's  $t$  test). At the left, a crypt-villus unit is shown and the different regions are indicated.

detected beyond 7 dpi in any part of the small intestinal epithelium. Analysis of adjacent sections revealed that the localization of NSP4 RNA and protein within the small intestinal epithelium correlated well and matched with that of the structural proteins (data not shown). Viral replication was not observed in the crypt compartment at any time during infection, and replication was confined solely to the villus epithelium. No rotavirus structural proteins (data not shown) or NSP4 mRNA or protein could be detected in the vacuoles at any time point. Quantitatively, very low expression of NSP4 mRNA was first observed in gut homogenates of the jejunum at 6 hpi (Fig. 3C). In agreement with the histological data, two peaks of viral replication were observed in both the jejunum and ileum. At 1 dpi there was a first peak of NSP4 mRNA expression. Expression was low at 2 dpi, and a second peak of replication was observed at 4 dpi. At 1 dpi, expression of NSP4 mRNA was statistically significantly higher in the ileum than in the jejunum. Quantitative data of rotavirus structural protein expression in gut homogenates correlated well with the expression of NSP4 mRNA (Fig. 3D). Some animals did not shed rotavirus at 1 dpi (Fig. 1). However, NSP4 mRNA and rotavirus structural protein expression was observed in the duodenum and jejunum, but not the ileum, of these animals (data not shown). Rotavirus antigen was not detected in any section of the small intestine of control mice.

**The pattern of epithelial vacuolization is more extensive than the pattern of replicating virus.** To determine whether replicating virus and vacuolated cells were found in the same region along the villi, crypt-villus units in the jejunum were divided into five regions of equal length. The positions were scored from 1 to 5, representing the tips of the villi to the crypts, respectively (Fig. 4). As stated earlier, the first infected cells were observed at 6 hpi, and vacuolated cells were first observed at 1 dpi. At 1 and 2 dpi, infected cells were exclusively found in the upper halves of the villi. However, vacuolated cells were observed along the entire villi, even at the base of

the villi where no rotavirus was detected. At 4 dpi, infected and vacuolated cells were found in the same region. At 7 dpi, no virus antigen was detected, but occasionally there was still some vacuolization of the enterocytes in the upper villus regions. A very similar pattern of vacuolization and replicating virus was observed in the ileum (data not shown). Note that these scores do not present data on the severity of histological pathology but rather present information on where the pathology was observed.

**Villus and crypt length during rotavirus infection.** We wanted to examine whether villus atrophy occurred in our homologous rotavirus model. In control mice, villus length in the jejunum remained constant during development in the second week after birth (i.e., 6 hpi to 7 dpi) (Fig. 5A). Then, when the control mice were 17 and 21 days old (i.e., 10 and 14 dpi), villi became significantly shorter (74 to 78%) compared to the control length at 6 hpi to 7 dpi. In control mice, the crypts of the jejunum increased in depth by about 100% during development in the period between 1 and 3 weeks (i.e., 6 hpi to 14 dpi) after birth. During infection, villus atrophy was observed as villi in the jejunum were shortened to 69 to 75% (i.e., at 6 hpi to 4 dpi) of the control length. Villus lengths of infected and control mice were comparable at 7 to 14 dpi. Crypt depth increased from 6 hpi to 14 dpi in control as well as infected mice. During infection there was a trend toward an increased crypt depth at 1 (142%) and 2 (134%) dpi compared to control mice; however, this did not reach statistical significance. From days 4 to 14 crypt depth of infected mice was comparable to that in controls.

**Apoptosis and proliferation of intestinal epithelial cells are increased during rotavirus infection.** To analyze jejunal epithelial proliferation and apoptosis during the course of rotavirus infection, proliferating cells were identified by expression of PCNA and apoptotic cells were identified by expression of cleaved caspase-3. In control animals, proliferating cells were almost exclusively observed in the crypt compartment (Fig.

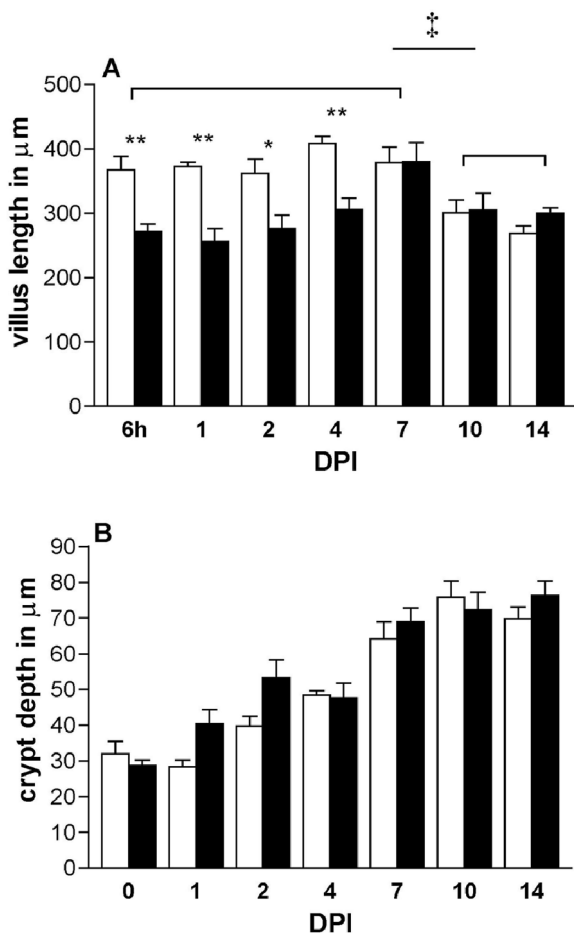


FIG. 5. Villus length (A) and crypt depth (B) in the jejunum of control mice (open bars) and during rotavirus infection (solid bars). Data from three to five animals at each time point are expressed as mean villus height and mean crypt depth  $\pm$  SEM (error bars). \* and \*\*,  $P < 0.05$  and  $P < 0.01$  (Student's  $t$  test). Controls at 6 and 7 dpi were compared to controls at 10 and 14 dpi and analyzed by analysis of variance followed by an unpaired  $t$  test ( $\ddagger$ ,  $P < 0.05$ ).

6A). However, in infected animals at 1 and 2 dpi, proliferating cells were abundantly covering the crypt epithelium and reached up to two-thirds of the length of the villi (Fig. 6B). The number of proliferating cells was strongly increased at 1 (153%) and 2 (206%) dpi but returned to control numbers from 4 to 14 dpi (Fig. 6E). Note that the number of proliferating cells in control animals gradually declined during development in the second week after birth. Apoptotic cells were rarely observed in control animals (Fig. 6C). During infection, apoptotic cells were particularly observed in the upper parts of the villi (Fig. 6D). Quantitative analysis of the number of cleaved caspase-3-positive cells showed that apoptosis follows the course of infection (Fig. 6F). At 1 and 4 dpi, there was a strong increase in the number of apoptotic cells. At 2 dpi, the number of apoptotic cells was not increased. Apoptosis was still slightly but significantly increased at 7 dpi but thereafter (at 10 and 14 dpi) normalized.

**Rotavirus infection alters epithelial cell migration kinetics in mouse small intestine.** As rotavirus infection caused increased epithelial proliferation as well as apoptosis, we wanted

to investigate the effects of infection on intestinal epithelial cell migration kinetics. Cell kinetics were analyzed through detection of incorporated BrdU that was injected at time zero, just before inoculation. The position of the foremost as well as least-progressed BrdU-labeled cells in a crypt-villus unit in the ileum was expressed as the number of cell positions from the crypt-villus boundary. There was no significant difference in the number of cells that had incorporated BrdU during the first 6 h after inoculation (data not shown). At 6 hpi, BrdU-positive cells in control and infected animals were restricted to the crypt compartment (Fig. 7). At 1 dpi, there was no difference between the positions of BrdU-labeled cells in infected and control animals. From 2 to 7 dpi, BrdU-positive cells in infected animals migrated significantly faster up the villi than in the respective controls. During infection, also the number of cell positions between the foremost cells and least-advanced cells was increased at 2 dpi. In control animals, BrdU-labeled cells were observed until 7 dpi. However, in infected animals, most of the BrdU-labeled cells were lost from the tips of the villi already at 4 dpi.

**Analysis of enterocyte gene expression in mouse small intestine during infection.** In order to examine enterocyte gene expression during rotavirus infection, we analyzed serial small intestinal sections (jejunum) by in situ hybridization. As markers for enterocyte gene expression we used lactase (the brush border protein that hydrolyzes the milk sugar lactose), SGLT1 (the brush border protein involved in the uptake of sodium, glucose, and water), and L-FABP (a cytoplasmic protein involved in fatty acid metabolism). L-FABP (Fig. 8C), SGLT1 (Fig. 8G), and beta-actin mRNA (data not shown) expression was detected in all enterocytes along the entire small intestinal villi of control animals. At 1 dpi, there was massive expression of NSP4 mRNA in the upper halves of the intestinal villi (Fig. 8A). In cells and areas on the villi that were NSP4 positive, there was an apparent downregulation of enterocyte (L-FABP and SGLT1) and housekeeping (beta-actin) mRNA expression (Fig. 8B, F, and E). At subsequent days after inoculation, this phenomenon was also observed, although not as prominently as it was during the first replication peak at 1 dpi. During infection, lactase mRNA expression followed the same pattern as SGLT1 and L-FABP mRNA expression (data not shown).

To examine whether enterocyte-specific gene expression in the jejunum was also quantitatively affected during infection, expression of lactase-, L-FABP-, and SGLT1 mRNA was assessed by RNA spot blotting. Since the expression of the housekeeping gene beta-actin was also affected by rotavirus infection, the amount of RNA spotted was corrected for GAPDH mRNA and 28S rRNA expression. Only data from spot blots normalized to GAPDH mRNA are shown, since spot blots normalized to 28S rRNA gave very similar results. Already at 6 hpi, all three markers were downregulated (Fig. 9). During massive viral replication at 1 dpi, mRNA levels were decreased to 15 to 22% of control levels. The mRNA levels were significantly decreased until 7 dpi (L-FABP and SGLT1) and 10 dpi (lactase). Notice that at 4 dpi, when there was a second peak of viral replication, no second decline of marker mRNA levels was observed. This suggests that mRNA levels in the remaining cells on the villi had increased at this time point.

In addition to mRNA expression, SGLT1 protein expression was examined by immunohistochemistry. In the jejunum of



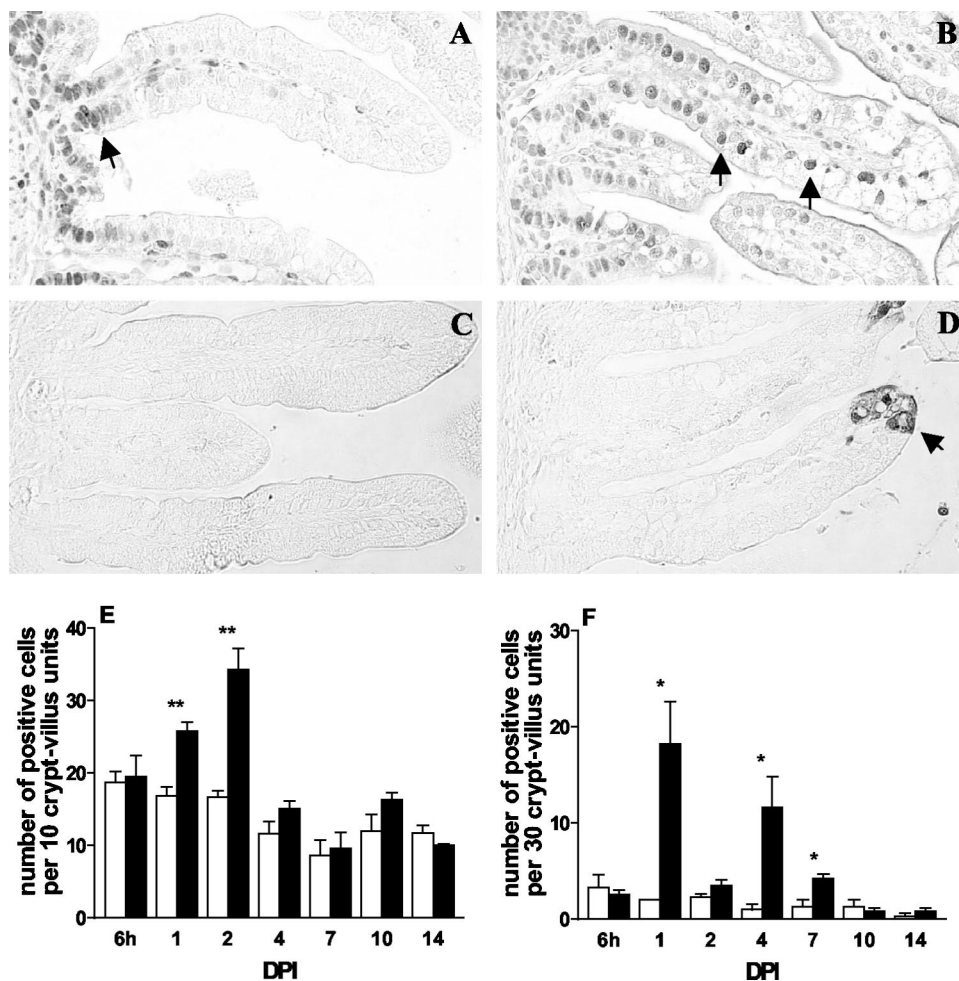


FIG. 6. Proliferation and apoptosis in jejunum during rotavirus infection as analyzed by staining of PCNA and cleaved caspase-3, respectively. (A) In control animals, proliferating cells were exclusively found in the crypt compartment (arrow). (B) In infected animals at 1 dpi, proliferating cells were observed on up to two-thirds of the length of the villi (arrows). (E) The numbers of proliferating cells in infected animals were strongly increased at 1 and 2 dpi (solid bars) and were comparable to control numbers (open bars) between 4 and 14 dpi (E). (C and F) Apoptotic cells were rarely observed in control animals (open bars). During infection at 1 dpi, however, apoptotic cells were abundantly observed at the villus tips (D) (arrow), and the numbers of apoptotic cells were significantly increased at 1, 4, and 7 dpi (F) (solid bars). \* and \*\*,  $P < 0.05$  and  $P < 0.01$  (Student's *t* test). Error bars, SEM. Original magnification,  $\times 250$ .

control animals, SGLT1 membrane protein was expressed in the enterocyte brush border (Fig. 8D). During rotavirus infection at 1 dpi, SGLT1 expression was almost completely lost from the brush border of enterocytes along the villi (Fig. 8H). Expression of SGLT1 protein was largely recovered by 4 dpi and was completely recovered by 7 dpi (data not shown). Lactase and L-FABP protein expression was also affected by rotavirus infection, and expression largely followed the pattern seen for SGLT1 (data not shown).

## DISCUSSION

In this study, we infected suckling mice with a homologous rotavirus strain. All phenomena that are presented in this work were observed in at least two independent experiments.

Mice developed diarrhea over a period of 5 days, starting at 1 day after inoculation. The onset of diarrhea coincided with the onset of viral shedding; however, rotavirus antigen was shed for a

total period of 10 days maximum. This means that after 5 to 10 dpi, virus antigen was shed, while no diarrheal illness occurred. Viral antigen in small intestinal tissue, however, was only observed until 4 dpi, indicating that diarrhea correlated with the presence of replicating virus in the intestinal tissue.

Two peaks of viral replication in small intestinal tissue were observed at 1 and 4 dpi. The occurrence of two antigen peaks during homologous (murine) rotavirus infection is in agreement with electron microscopic studies in infant mice (43, 61). The second peak of viral replication at 4 dpi is most likely caused by infection of newly formed cells, since we show that most BrdU-labeled cells, present during inoculation, were lost within 4 days.

During both peaks of infection, levels of NSP4 mRNA and structural rotavirus proteins were higher in the ileum than in the jejunum. Although some animals did not shed rotavirus at 1 dpi, replicating virus was observed in the duodenum and jejunum, but not ileum, of these animals (data not shown).

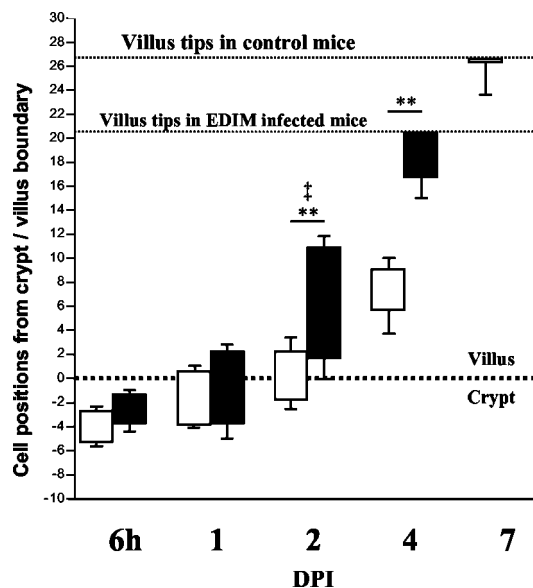


FIG. 7. Cell migration kinetics in the mouse small intestine (ileum) during rotavirus infection. Just before inoculation, mice were injected with BrdU. The positions of the foremost as well as least-progressed BrdU-labeled cells in each crypt-villus unit are expressed as the number of cell positions from the crypt-villus boundary (shown as a dotted line at 0 on the graph). At 6 hpi, BrdU-positive cells in control (open bars) and infected (closed bars) animals were restricted to the crypt compartment. From 2 to 7 dpi, BrdU-positive cells in infected animals migrated significantly higher up the villi than in respective controls (\*,  $P < 0.05$ ; \*\*,  $P < 0.01$ ). The number of cell positions between the foremost and least-advanced cells was also increased at 2 dpi (‡,  $P < 0.05$ ). However, in infected animals, BrdU-labeled cells were predominantly lost from the villi at 4 dpi.

These findings suggest that infection begins in the proximal small intestine but eventually is more severe in the distal small intestine at later stages during infection.

With respect to the exact timing of the induction of damage and viral replication, it appears that the initial load of viral inoculum is of particular importance. From previous experiments, we observed that when mice were inoculated with fewer ( $2 \times 10^3$  or  $5 \times 10^2$ ) FFU, the development of histological damage and the appearance of the first peak of viral replication were delayed by 1 day compared to those observed for mice inoculated with the high dose of  $2 \times 10^4$  FFU. Interestingly, the mice inoculated with the lower virus load eventually developed peaks of infection that were comparable with those of the higher load (unpublished data).

During infection at 1 to 7 dpi, large vacuoles were observed in enterocytes lining most of the surface of the villi in the small intestine. The vacuoles seemed largely devoid of rotavirus antigen as determined by immunohistochemistry. This observation is in agreement with other studies in mice and rats (20, 43, 46), although rotavirus particles were observed by electron microscopy to be associated with intracytoplasmic vacuoles in canine rotavirus-infected gnotobiotic dogs (27). At 1 and 2 dpi, many vacuolated cells were found lower on the villi than infected cells. Moreover, vacuolization was observed in many cells in which no NSP4 or structural proteins were detected, and cells that were strongly positive for rotavirus antigen seemed histologically undamaged. In agreement with other

studies, these findings suggest that there is no direct correlation between the occurrence and severity of vacuolization of the enterocytes and the presence of virus (8, 9, 43). The vacuoles do not stain for acid or neutral carbohydrates with alcian blue or PAS, respectively. Others found that the vacuoles in infected neonatal rats also did not contain neutral lipids (8). Therefore, the origin and nature of these vacuoles remain obscure.

It has been suggested that vacuolization is a late state of infection that precedes extrusion (9). However, the fact that the vacuolated cells were found lower on the villi than virus-infected cells at various time points during infection suggests that vacuolization is not directly caused by infection of these cells. Therefore, vacuolization might be caused by a systemic mechanism or by a secreted (viral) factor. One such viral factor is NSP4. After being secreted from infected cells, NSP4 is thought to mediate cell signaling by increasing intracellular calcium levels, leading to chloride secretion in uninfected cells (1).

In addition to the morphological damage, we analyzed the changes in epithelial homeostasis during rotavirus infection by studying epithelial proliferation, migration, and apoptosis. In our study, the rate of proliferation during infection was strongly increased at 1 and 2 dpi as indicated by increased numbers of PCNA-positive cells. Indications for increased proliferation rates in mice during rotavirus infection also come from studies showing that the activity of thymidine kinase is increased (10, 14, 43). Epithelial migration was also drastically increased as indicated by the BrdU labeling study. Overall, this led to an increase in epithelial cell turnover from 7 days in control mice to 4 days in infected mice.

To our knowledge, this is the first study to describe increased apoptosis during rotavirus infection *in vivo*. Apoptotic cells were mainly observed in the upper parts of the villi where most infected cells were observed. The number of apoptotic cells followed the course of infection. These findings indicate that rotavirus directly causes the increased apoptosis of villus enterocytes. In HT-29 human adenocarcinoma cells, SA11 rotavirus infection was also found to trigger apoptosis, and Superti et al. stated that the specific histological features of rotavirus infected enterocytes may be a consequence of virus-induced apoptosis (62). However, in our study most damaged and vacuolated cells were not caspase-3 positive and also were found lower on the villi than infected cells. Moreover, many apoptotic cells were not morphologically damaged upon histological examination. This suggests that vacuolization is not a direct consequence of apoptosis but rather precedes it.

Rotavirus infection in children can result in the occurrence of a flat mucosa with total villus atrophy (3), and the most-severe form of villus atrophy is observed in piglets, where small intestinal villi can be completely eroded (57). Villus atrophy in mice is mild compared to that observed in other mammalian species (3, 7, 35, 57, 60, 61). Villus atrophy in our model occurred as early as 6 hpi, before the onset of massive viral replication. At this stage of infection, no obvious histological damage or increased apoptosis was observed. The shortening of the villi is therefore possibly caused by an effect of infection on the smooth muscle cells or the subepithelial network of myofibroblasts within the villi. Speculatively this rapid villus contraction involves the enteric nervous system.



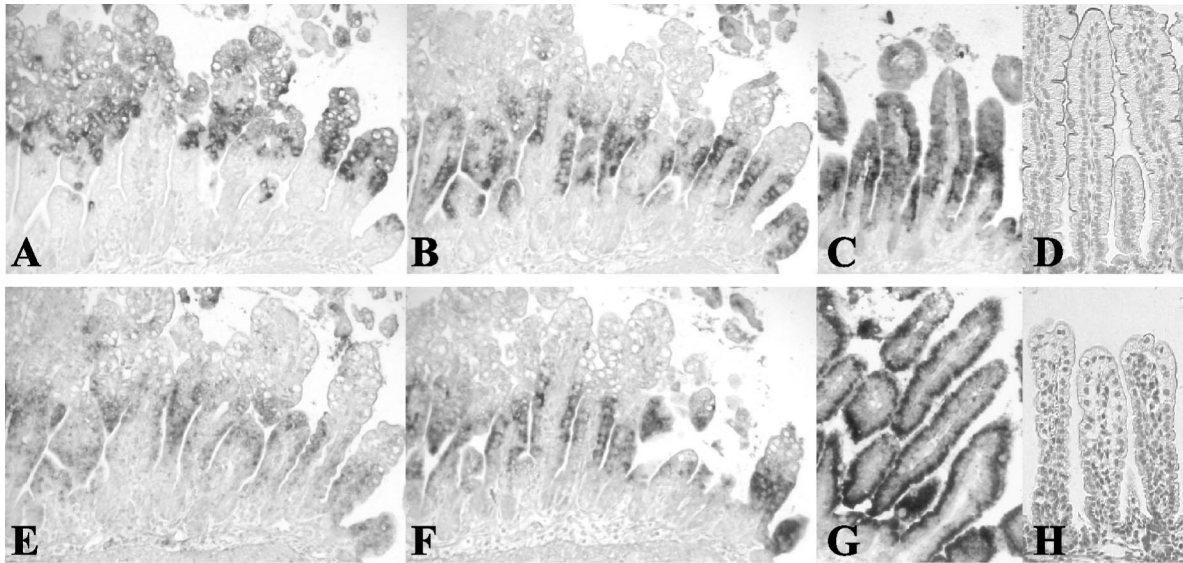


FIG. 8. Histological analysis of enterocyte gene expression during rotavirus infection. NSP4 (A), L-FABP (B), beta-actin (E), and SGLT1 (F) mRNA expression in serial small intestinal (jejunum) sections during rotavirus infection as examined by in situ hybridization (at 1 dpi). During massive expression of NSP4 in enterocytes in the upper halves of the villi at 1 dpi (A), enterocyte-specific L-FABP, beta-actin, and SGLT1 mRNA expression was downregulated in these cells (B, E, and F). In control animals, L-FABP mRNA (C), SGLT1 mRNA (G), and beta-actin mRNA (data not shown) were expressed in all enterocytes along the entire villi. (D) SGLT1 protein was observed in the brush border of control animals. (H) At 1 dpi, expression of SGLT1 protein was almost completely lost in infected animals. Magnifications:  $\times 150$  (A, B, C, E, F, and G) and  $\times 175$  (D and H).

On the subsequent days, villus atrophy is likely attributed to the strong increase in apoptosis. One of the most plausible explanations for the relatively minor villus atrophy in mice is our observation of a very strong increase in the number of proliferating cells and cellular migration that potentially counteracts the increased number of shed and apoptotic cells. The pathogenesis of this enhanced proliferation is unknown, but a negative feedback from mature villus epithelium has been postulated (30, 51, 56). The shedding of differentiated enterocytes

may result in a deficient negative feedback of mature enterocytes, resulting in enhanced proliferation. In our model, the small intestinal epithelium likely responds to the increased loss of epithelial cells by enhancing the replacement of these cells through induction of proliferation in the crypts, as well as at the base of the villi. As has been proposed by others, we think that the basal region of the villi might constructively contribute to the process of enhanced renewal of villus cells (43, 52).

We studied the expression of enterocyte-specific lactase, L-

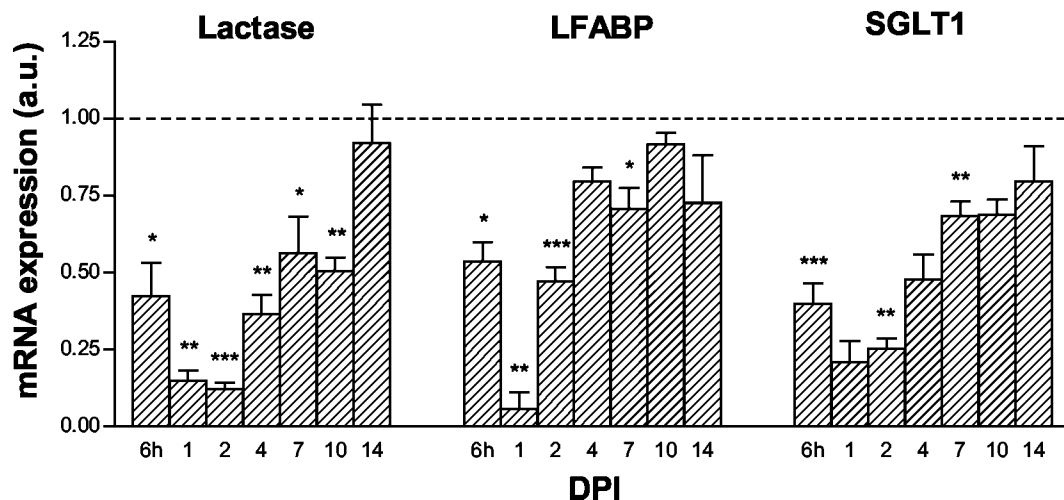


FIG. 9. Quantitative analyses of enterocyte mRNA expression during rotavirus infection. Control values per day were arbitrarily set at a relative expression of 1 and are represented as a dotted line. At 6 hpi, enterocyte mRNA levels in the jejunum of infected animals were decreased compared to those of controls (dashed line). mRNA levels remained significantly decreased until 7 dpi (L-FABP and SGLT1) and 10 dpi (lactase). The amount of RNA spotted was corrected for GAPDH mRNA expression. Symbols: \*,  $P < 0.05$ ; \*\*,  $P < 0.01$ ; \*\*\*,  $P < 0.001$  (versus control using Student's *t* test). Error bars, SEM; a.u., arbitrary units.

FABP, and SGLT1 mRNAs as markers for the absorptive and metabolic functions of the enterocytes. Lactase is essential for the hydrolysis of lactose (65), the most important sugar in milk. L-FABP is a protein that is involved in the uptake and intracellular transport of fatty acids (25), and SGLT1 is a glucose cotransporter involved in the uptake of glucose, salts, and water (15). Already after 6 h, we observed reduced levels of these enterocyte-specific mRNAs. The downregulation of these genes in vivo persisted till 10 dpi. The most prominent effect of viral infection was observed at 1 dpi. At this time point there was a very distinct downregulation of enterocyte gene expression in cells that harbored replicating virus. Enterocyte-specific protein levels were also reduced at days 1 and 2 dpi, following the reduced levels of the cognate mRNAs. This is in agreement with an earlier study where mice were infected with a homologous (murine) rotavirus; lactase and alkaline phosphatase activities were reduced, whereas sucrase-isomaltase activity showed a precocious maturation (10). Katyal and co-workers found that there was a reduced amino acid (leucine) uptake in the jejunum and ileum of mice infected with a homologous rotavirus (29). In rabbits, rotavirus infection was shown to impair intestinal brush border membrane  $\text{Na}^+$  solute cotransport activities of SGLT1. This effect was found to be mediated by a direct inhibiting effect of NSP4 on SGLT1 and not by means of reduced levels of SGLT1 in brush border vesicles (21, 22). Our data, however, show that these observed reductions of  $\text{Na}^+$  solute cotransport activities, at least in mice, are probably caused not only by a direct inhibitory effect of rotavirus proteins (NSP4) on SGLT1 activity but also by reduced levels of SGLT1 transcripts and SGLT1 protein in the brush border of enterocytes. So from our study, it seems that a reduced amount of the transporter (SGLT1) in the brush border membrane of enterocytes might be one of the mechanisms underlying the reduced  $\text{Na}^+$  solute transport activity observed during rotavirus infection in rabbits (21).

Together these findings suggest that the enterocyte absorptive and metabolic capacities are affected, which might contribute to pathogenesis of rotavirus infection.

Many viruses (human immunodeficiency virus, influenza virus, poliovirus, adenovirus, and herpes simplex virus) are known to interfere with the host cell translational machinery and shut off gene expression in a variety of ways (4, 33, 36, 39, 68). The rotavirus NSP3 is capable of inducing the shutoff of host cell translation during in vitro rotavirus infection, by interacting with the eukaryotic initiation factor 4GI (eIF4GI), which is part of the eIF4F holoenzyme complex (44). Since eIF4F modulates mRNA stability (47), the shutoff of enterocyte gene expression during rotavirus infection we observed here in vivo might also be mediated by NSP3. Furthermore, we hypothesize that NSP3 could mediate this shutoff by removing eIF4F from cellular mRNA, resulting in decreased stability of these mRNAs and subsequently a decreased translation. However, this shutoff might not be absolute, since several in vitro studies indicate an upregulation of specific genes in infected cells (13, 69).

Based on the present data, we suggest that the hypothesis of Hamilton and colleagues (23, 31, 50) used to explain one of the mechanisms for rotavirus-induced diarrhea—that is, decreased solute absorption and water reabsorption in the intestine through substitution of mature enterocytes by nontransporting

crypt cells—needs further refinement. In relation to the inhibitory effect of rotavirus on the absorptive function of the small intestinal epithelium, we propose that in addition to the direct inhibition of  $\text{Na}^+$  solute cotransport activities through NSP4, at least three sequential processes are implicated in this mechanism of rotavirus-induced diarrhea. (i) Early on during infection, enterocyte-specific gene expression is directly downregulated in infected cells at the mRNA level. This results in reduction of mature enterocyte-specific protein levels and thus in a functional less differentiated status relatively early during infection while there is still little histological damage. (ii) Mature enterocytes are lost from the villi through apoptosis and shedding. (iii) These mature enterocytes are replaced by immature and actively dividing cells.

In summary, we report that during a homologous rotavirus infection in mice, villus atrophy and an increase in crypt depth are accompanied by highly induced epithelial apoptotic and proliferation rates. Epithelial cell turnover was increased from 7 days in controls to 4 days in infected mice, indicating that the second peak of viral replication was most likely caused by infection of newly synthesized epithelial cells. Rotavirus infection caused a downregulation of enterocyte-specific gene expression in vivo in infected cells. This suggests that rotavirus infection causes a shutoff of endogenous gene expression in favor of viral gene expression. The shutoff of enterocyte-specific gene expression, together with the loss of mature enterocytes through apoptosis and the replacement of these cells by less differentiated dividing cells, likely leads to a defective absorptive function of the intestinal epithelium, which contributes to rotavirus pathogenesis.

#### ACKNOWLEDGMENTS

We thank R. Ward for donating the EDIM mouse rotavirus strain. We thank A. Quaroni and B. Hirayama for kindly providing the anti-rat lactase antibody and the anti-rabbit SGLT1 antibody, respectively. We are grateful to J. Gordon for providing both the anti-rat L-FABP antibody and the rat L-FABP probe, C. F. Burant for providing the rat SGLT1 probe, and S. D. Krasinski for donating the beta-actin probe. We thank G. van Amerongen, M. van der Sluis, and D. J. P. M. van Nispen for excellent technical assistance.

This work was supported by grants from the Sophia Foundation for Medical Research and The Netherlands Digestive Diseases Foundation.

#### REFERENCES

- Ball, J. M., P. Tian, C. Q. Zeng, A. P. Morris, and M. K. Estes. 1996. Age-dependent diarrhea induced by a rotaviral nonstructural glycoprotein. *Science* 272:101–104.
- Bell, L. M., H. F. Clark, E. A. O'Brien, M. J. Kornstein, S. A. Plotkin, and P. A. Offit. 1987. Gastroenteritis caused by human rotaviruses (serotype three) in a suckling mouse model. *Proc. Soc. Exp. Biol. Med.* 184:127–132.
- Bishop, R. F., G. P. Davidson, I. H. Holmes, and B. J. Ruck. 1973. Virus particles in epithelial cells of duodenal mucosa from children with acute non-bacterial gastroenteritis. *Lancet* ii:1281–1283.
- Black, T. L., G. N. Barber, and M. G. Katze. 1993. Degradation of the interferon-induced 68,000- $M_r$  protein kinase by poliovirus requires RNA. *J. Virol.* 67:791–800.
- Both, G. W., J. S. Mattick, and A. R. Bellamy. 1983. Serotype-specific glycoprotein of simian 11 rotavirus: coding assignment and gene sequence. *Proc. Natl. Acad. Sci. USA* 80:3091–3095.
- Buller, H. A., M. J. Kothe, D. A. Goldman, S. A. Grubman, W. V. Sasak, P. T. Matsudaira, R. K. Montgomery, and R. J. Grand. 1990. Coordinate expression of lactase-phlorizin hydrolase mRNA and enzyme levels in rat intestine during development. *J. Biol. Chem.* 265:6978–6983.
- Burns, J. W., A. A. Krishnaney, P. T. Vo, R. V. Rouse, L. J. Anderson, and H. B. Greenberg. 1995. Analyses of homologous rotavirus infection in the mouse model. *Virology* 207:143–153.
- Ciarlet, M., M. E. Conner, M. J. Finegold, and M. K. Estes. 2002. Group A

- rotavirus infection and age-dependent diarrheal disease in rats: a new animal model to study the pathophysiology of rotavirus infection. *J. Virol.* **76**:41–57.
9. **Coelho, K. I., A. S. Bryden, C. H. Hall, and T. H. Flewett.** 1981. Pathology of rotavirus infection in suckling mice: a study by conventional histology, immunofluorescence, ultrathin sections, and scanning electron microscopy. *Ultrastruct. Pathol.* **2**:59–80.
  10. **Collins, J., W. G. Starkey, T. S. Wallis, G. J. Clarke, K. J. Worton, A. J. Spencer, S. J. Haddon, M. P. Osborne, D. C. Candy, and J. Stephen.** 1988. Intestinal enzyme profiles in normal and rotavirus-infected mice. *J. Pediatr. Gastroenterol. Nutr.* **7**:264–272.
  11. **Corpe, C. P., and C. F. Burant.** 1996. Hexose transporter expression in rat small intestine: effect of diet on diurnal variations. *Am. J. Physiol.* **271**:G211–G216.
  12. **Cox, K. H., D. V. DeLeon, L. M. Angerer, and R. C. Angerer.** 1984. Detection of mRNAs in sea urchin embryos by in situ hybridization using asymmetric RNA probes. *Dev. Biol.* **101**:485–502.
  13. **Cuadras, M. A., D. A. Feigelstock, S. An, and H. B. Greenberg.** 2002. Gene expression pattern in Caco-2 cells following rotavirus infection. *J. Virol.* **76**:4467–4482.
  14. **Davidson, G. P., D. G. Gall, M. Petric, D. G. Butler, and J. R. Hamilton.** 1977. Hum. rotavirus enteritis induced in conventional piglets. Intestinal structure and transport. *J. Clin. Invest.* **60**:1402–1409.
  15. **Dekker, J., A. W. C. Einerhand, and H. A. Büller.** 2002. Carbohydrate malabsorption, p. 339–374. *In* C. H. Lifschitz (ed.), *Pediatric gastroenterology and nutrition in clinical practice*. Marcel Dekker Inc., New York, N.Y.
  16. **Estes, M. K.** 2001. Rotaviruses and their replication, p. 1747–1785. *In* D. M. Knipe and P. M. Howley (ed.), *Fields virology*. Lippincott-Raven Publishers, Philadelphia, Pa.
  17. **Estes, M. K., and J. Cohen.** 1989. Rotavirus structure and function. *Microbiol. Rev.* **53**:410–449.
  18. **Feng, N., M. A. Franco, and H. B. Greenberg.** 1997. Murine model of rotavirus infection. *Adv. Exp. Med. Biol.* **412**:233–240.
  19. **Gouvea, V. S., A. A. Alencar, O. M. Barth, L. de Castro, A. M. Fialho, H. P. Araujo, S. Majerowicz, and H. G. Pereira.** 1986. Diarrhoea in mice infected with a human rotavirus. *J. Gen. Virol.* **67**:577–581.
  20. **Guerin-Danan, C., J. C. Meslin, F. Lambre, A. Charpilienne, M. Serezat, C. Bouley, J. Cohen, and C. Andrieux.** 1998. Development of a heterologous model in germfree suckling rats for studies of rotavirus diarrhea. *J. Virol.* **72**:9298–9302.
  21. **Halaihel, N., V. Lievin, F. Alvarado, and M. Vasseur.** 2000. Rotavirus infection impairs intestinal brush-border membrane Na<sup>+</sup>-solute cotransport activities in young rabbits. *Am. J. Physiol. Gastrointest. Liver Physiol.* **279**:G587–G596.
  22. **Halaihel, N., V. Lievin, J. M. Ball, M. K. Estes, F. Alvarado, and M. Vasseur.** 2000. Direct inhibitory effect of rotavirus NSP4(114-135) peptide on the Na<sup>+</sup>-D-glucose symporter of rabbit intestinal brush border membrane. *J. Virol.* **74**:9464–9470.
  23. **Hamilton, J. R.** 1988. Viral enteritis. *Pediatr. Clin. N. Am.* **35**:89–101.
  24. **Hirayama, B. A., M. P. Lostao, M. Panayotova-Heiermann, D. D. Loo, E. Turk, and E. M. Wright.** 1996. Kinetic and specificity differences between rat, human, and rabbit Na<sup>+</sup>-glucose cotransporters (SGLT-1). *Am. J. Physiol.* **270**:G919–G926.
  25. **Hsu, K. T., and J. Storch.** 1996. Fatty acid transfer from liver and intestinal fatty acid-binding proteins to membranes occurs by different mechanisms. *J. Biol. Chem.* **271**:13317–13323.
  26. **Institute of Medicine.** 1986. New vaccine development: establishing priorities, vol. II. Diseases of importance in developing countries. National Academies Press, Washington, D.C.
  27. **Johnson, C. A., T. G. Snider, 3rd, W. G. Henk, and R. W. Fulton.** 1986. A scanning and transmission electron microscopic study of rotavirus-induced intestinal lesions in neonatal gnotobiotic dogs. *Vet. Pathol.* **23**:443–453.
  28. **Kapikian, A. Z., and R. M. Chanock.** 1990. Rotaviruses, p. 1353–1404. *In* B. N. Fields, D. M. Knipe, R. M. Chanock, M. S. Hirsch, J. L. Melnick, and B. Roizman (ed.), *Virology*, 2nd ed. Raven Press, New York, N.Y.
  29. **Katyal, R., S. V. Rana, K. Vaiphei, S. Ohja, K. Singh, and V. Singh.** 1999. Effect of rotavirus infection on small gut pathophysiology in a mouse model. *J. Gastroenterol. Hepatol.* **14**:779–784.
  30. **Keenan, K. P., H. R. Jervis, R. H. Marchwicki, and L. N. Binn.** 1976. Intestinal infection of neonatal dogs with canine coronavirus 1-71: studies by virologic, histologic, histochemical, and immunofluorescent techniques. *Am. J. Vet. Res.* **37**:247–256.
  31. **Keljo, D. J., R. J. MacLeod, M. H. Perdue, D. G. Butler, and J. R. Hamilton.** 1985. D-Glucose transport in piglet jejunal brush-border membranes: insights from a disease model. *Am. J. Physiol.* **249**:G751–G760.
  32. **Krasinski, S. D., G. Estrada, K. Y. Yeh, M. Yeh, P. G. Traber, E. H. Rings, H. A. Buller, M. Verhave, R. K. Montgomery, and R. J. Grand.** 1994. Transcriptional regulation of intestinal hydrolase biosynthesis during postnatal development in rats. *Am. J. Physiol.* **267**:G584–G594.
  33. **Kwong, A. D., and N. Frenkel.** 1987. Herpes simplex virus-infected cells contain a function(s) that destabilizes both host and viral mRNAs. *Proc. Natl. Acad. Sci. USA* **84**:1926–1930.
  34. **Lindenbergh-Kortleve, D. J., R. R. Rosato, J. W. van Neck, J. Nauta, M. van Kleffens, C. Groffen, E. C. Zwarthoff, and S. L. Drop.** 1997. Gene expression of the insulin-like growth factor system during mouse kidney development. *Mol. Cell. Endocrinol.* **132**:81–91.
  35. **Little, L. M., and J. A. Shadduck.** 1982. Pathogenesis of rotavirus infection in mice. *Infect. Immun.* **38**:755–763.
  36. **Lu, Y., M. Wambach, M. G. Katze, and R. M. Krug.** 1995. Binding of the influenza virus NS1 protein to double-stranded RNA inhibits the activation of the protein kinase that phosphorylates the eIF-2 translation initiation factor. *Virology* **214**:222–228.
  37. **Lundgren, O., A. T. Peregrin, K. Persson, S. Kordasti, I. Uhnöo, and L. Svensson.** 2000. Role of the enteric nervous system in the fluid and electrolyte secretion of rotavirus diarrhea. *Science* **287**:491–495.
  38. **Majerowicz, S., C. F. Kubelka, P. Stephens, and O. M. Barth.** 1994. Ultrastructural study on experimental infection of rotavirus in a murine heterologous model. *Mem. Inst. Oswaldo Cruz* **89**:395–402.
  39. **Mathews, M. B., and T. Shenk.** 1991. Adenovirus virus-associated RNA and translation control. *J. Virol.* **65**:5657–5662.
  40. **McNeal, M. M., K. S. Barone, M. N. Rae, and R. L. Ward.** 1995. Effector functions of antibody and CD8<sup>+</sup> cells in resolution of rotavirus infection and protection against reinfection in mice. *Virology* **214**:387–397.
  41. **Mebius, C. A., M. Kono, N. R. Underdahl, and M. J. Twiehaus.** 1971. Cell culture propagation of neonatal calf diarrhea (scours) virus. *Can. Vet. J.* **12**:69–72.
  42. **Offit, P. A., H. F. Clark, M. J. Kornstein, and S. A. Plotkin.** 1984. A murine model for oral infection with a primate rotavirus (simian SA11). *J. Virol.* **51**:233–236.
  43. **Osborne, M. P., S. J. Haddon, A. J. Spencer, J. Collins, W. G. Starkey, T. S. Wallis, G. J. Clarke, K. J. Worton, D. C. Candy, and J. Stephen.** 1988. An electron microscopic investigation of time-related changes in the intestine of neonatal mice infected with murine rotavirus. *J. Pediatr. Gastroenterol. Nutr.* **7**:236–248.
  44. **Piron, M., P. Vende, J. Cohen, and D. Poncet.** 1998. Rotavirus RNA-binding protein NSP3 interacts with eIF4G1 and evicts the poly(A) binding protein from eIF4F. *EMBO J.* **17**:5811–5821.
  45. **Quaroni, A., and K. J. Isselbacher.** 1985. Study of intestinal cell differentiation with monoclonal antibodies to intestinal cell surface components. *Dev. Biol.* **111**:267–279.
  46. **Ramig, R. F.** 1988. The effects of host age, virus dose, and virus strain on heterologous rotavirus infection of suckling mice. *Microb. Pathog.* **4**:189–202.
  47. **Ramirez, C. V., C. Vilela, K. Berthelot, and J. E. McCarthy.** 2002. Modulation of eukaryotic mRNA stability via the Cap-binding translation complex eIF4F. *J. Mol. Biol.* **318**:951–962.
  48. **Renes, I. B., J. A. Boshuizen, D. J. Van Nispen, N. P. Bulting, H. A. Buller, J. Dekker, and A. W. Einerhand.** 2002. Alterations in Muc2 biosynthesis and secretion during dextran sulfate sodium-induced colitis. *Am. J. Physiol. Gastrointest. Liver Physiol.* **282**:G382–G389.
  49. **Renes, I. B., M. Verburg, N. P. Bulting, S. Ferdinandusse, H. A. Buller, J. Dekker, and A. W. C. Einerhand.** 2002. Protection of the Peyer's patch associated crypt and villus epithelium against methotrexate-induced damage is based on its distinct regulation of proliferation. *J. Pathol.* **198**:60–68.
  50. **Rhoads, J. M., R. J. MacLeod, and J. R. Hamilton.** 1989. Diminished brush border membrane Na-dependent L-alanine transport in acute viral enteritis in piglets. *J. Pediatr. Gastroenterol. Nutr.* **9**:225–231.
  51. **Rijke, R. P., W. R. Hanson, H. M. Plaisier, and J. W. Osborne.** 1976. The effect of ischemic villus cell damage on crypt cell proliferation in the small intestine: evidence for a feedback control mechanism. *Gastroenterology* **71**:786–792.
  52. **Robinson, J. W., V. Mirkovitch, B. Winistorfer, and F. Saegesser.** 1981. Response of the intestinal mucosa to ischaemia. *Gut* **22**:512–527.
  53. **Rollo, E. E., K. P. Kumar, N. P. Bulting, J. Cohen, J. Angel, H. B. Greenberg, R. Sheth, J. Anderson, B. Oh, S. J. Hempson, E. R. Mackow, and R. D. Shaw.** 1999. The epithelial cell response to rotavirus infection. *J. Immunol.* **163**:4442–4452.
  54. **Roth, K. A., J. M. Hertz, and J. I. Gordon.** 1990. Mapping enteroendocrine cell populations in transgenic mice reveals an unexpected degree of complexity in cellular differentiation within the gastrointestinal tract. *J. Cell Biol.* **110**:1791–1801.
  55. **Salim, A. F., A. D. Phillips, and M. J. Farthing.** 1990. Pathogenesis of gut virus infection. *Bailliere's Clin. Gastroenterol.* **4**:593–607.
  56. **Saxena, S. K., J. S. Thompson, D. A. Crouse, and J. G. Sharp.** 1991. Epithelial cell proliferation and uptake of radiolabeled urogastrone in the intestinal tissues following abdominal irradiation in the mouse. *Radiat. Res.* **128**:37–42.
  57. **Shepherd, R. W., D. G. Butler, E. Cutz, D. G. Gall, and J. R. Hamilton.** 1979. The mucosal lesion in viral enteritis. Extent and dynamics of the epithelial response to virus invasion in transmissible gastroenteritis of piglets. *Gastroenterology* **76**:770–777.
  58. **Simon, T. C., K. A. Roth, and J. I. Gordon.** 1993. Use of transgenic mice to map cis-acting elements in the liver fatty acid-binding protein gene (Fabpl)



- that regulate its cell lineage-specific, differentiation-dependent, and spatial patterns of expression in the gut epithelium and in the liver acinus. *J. Biol. Chem.* **268**:18345–18358.
59. **Snodgrass, D. R., K. W. Angus, and E. W. Gray.** 1977. Rotavirus infection in lambs: pathogenesis and pathology. *Arch. Virol.* **55**:263–274.
  60. **Snodgrass, D. R., A. Ferguson, F. Allan, K. W. Angus, and B. Mitchell.** 1979. Small intestinal morphology and epithelial cell kinetics in lamb rotavirus infections. *Gastroenterology* **76**:477–481.
  61. **Starkey, W. G., J. Collins, T. S. Wallis, G. J. Clarke, A. J. Spencer, S. J. Haddon, M. P. Osborne, D. C. Candy, and J. Stephen.** 1986. Kinetics, tissue specificity and pathological changes in murine rotavirus infection of mice. *J. Gen. Virol.* **67**:2625–2634.
  62. **Superti, F., M. G. Ammendolia, A. Tinari, B. Bucci, A. M. Giammarioli, G. Rainaldi, R. Rivabene, and G. Donelli.** 1996. Induction of apoptosis in HT-29 cells infected with SA-11 rotavirus. *J. Med. Virol.* **50**:325–334.
  63. **Tytgat, K. M., H. A. Buller, F. J. Opdam, Y. S. Kim, A. W. Einerhand, and J. Dekker.** 1994. Biosynthesis of human colonic mucin: Muc2 is the prominent secretory mucin. *Gastroenterology* **107**:1352–1363.
  64. **Uhnou, I., T. Dharakul, M. Riepenhoff-Talty, and P. L. Ogra.** 1988. Immunological aspects of interaction between rotavirus and the intestine in infancy. *Immunol. Cell Biol.* **66**:135–145.
  65. **Van Beers, E. H., H. A. Buller, R. J. Grand, A. W. Einerhand, and J. Dekker.** 1995. Intestinal brush border glycohydrolases: structure, function, and development. *Crit. Rev. Biochem. Mol. Biol.* **30**:197–262.
  66. **Verburg, M., I. B. Renes, H. P. Meijer, J. A. Taminiau, H. A. Buller, A. W. Einerhand, and J. Dekker.** 2000. Selective sparing of goblet cells and paneth cells in the intestine of methotrexate-treated rats. *Am. J. Physiol. Gastrointest. Liver Physiol.* **279**:G1037–G1047.
  67. **Ward, R. L., M. M. McNeal, and J. F. Sheridan.** 1990. Development of an adult mouse model for studies on protection against rotavirus. *J. Virol.* **64**:5070–5075.
  68. **Xiao, H., C. Neuveut, M. Benkirane, and K. T. Jeang.** 1998. Interaction of the second coding exon of Tat with human EF-1 delta delineates a mechanism for HIV-1-mediated shut-off of host mRNA translation. *Biochem. Biophys. Res. Commun.* **244**:384–389.
  69. **Xu, A., A. R. Bellamy, and J. A. Taylor.** 1998. BiP (GRP78) and endoplasmic reticulum (GRP94) are induced following rotavirus infection and bind transiently to an endoplasmic reticulum-localized virion component. *J. Virol.* **72**:9865–9872.